EasyChair Preprint

№ 4379

Nonlocal Adaptive Biharmonic Regularizer for Image Restoration

Ying Wen and Luminita Vese

October 12, 2020

Nonlocal Adaptive Biharmonic Regularizer for Image Restoration

Ying Wen[1][0000−0002−6354−1168] and Luminita A. Vese[2][0000−0003−3002−9982]

[1] School of Mathematics, Harbin Institute of Technology, Harbin, China.
wenyinghitmath@gmail.com
[2] Department of Mathematics, University of California, Los Angeles, CA, USA
lvese@math.ucla.edu

Abstract. In this paper, we propose a nonlocal adaptive biharmonic regularization term for image denoising and restoration, combining the advantages of fourth order models (without the staircase effect while preserving slopes) and nonlocal methods (preserving texture). For its numerical solution, we employ the L^2 gradient descent and finite difference methods to design explicit, semi-implicit, and implicit schemes. Numerical results for denoising and restoration are shown on synthetic images, real images, and texture images. Comparisons with local fourth order regularizer and the nonlocal total variation are made, which help illustrate the advantages of the proposed model.

Keywords: Nonlocal Method · Fourth Order · Image Restoration.

1 Introduction

Image denoising and restoration (denoising-deblurring) has always been an essential and challenging task in the fields of image processing and computer vision. In this paper, we propose a nonlocal higher order model to denoise and deblur images corrupted by Gaussian noise. Until now, there is a variety of methods developed to deal with denoising and restoration problems in the variational setting. Rudin, Osher, and Fatemi proposed the total variation regularization [1] which is remarkably effective at simultaneously preserving edges whilst smoothing away noise in flat regions, and it is widely applied to various research fields of computer vision. Perona and Malik proposed a partial differential equation based model for image denoising [2] which consists of a forward-backward diffusion process controlled by a diffusion coefficient to smooth noise and preserve edges. To overcome the staircase effect of second order partial differential equation methods, fourth order equations for image denoising have been employed. We mention the earlier work of Chambolle and Lions [3], of Chan, Marquina, and Mulet [4], of You and Kaveh [5], of Lysaker et al. [6], and of Hajiaboli [7]. These models can better preserve smooth regions and ramps, thus diminishing the staircase effect. These image denoising and restoration methods are based on local image operators. However, texture is nonlocal in nature and requires nonlocal information for efficient noise removal and image restoration. Following the nonlocal means

filter of Buades, Coll, and Morel [8], Gilboa and Osher proposed the nonlocal total variation regularization for image processing [9]. Their work utilized the nonlocal gradient and Laplacian to formulate variational-based methods for image denoising, inpainting, anomaly detection, and image-texture separation. In the work of Lou et al [10], the authors have extended the nonlocal total variation model to image restoration (simultaneous denoising and deblurring). Other second-order nonlocal methods for image restoration have been proposed in [11].

Here we propose a nonlocal fourth order model for image denoising and restoration. The model can be seen as a nonlocal version of the biharmonic operator. Also, two versions are considered, an isotropic and an anisotropic one. In the anisotropic case, an adaptive coefficient is used, depending on the input image, that helps preserve edges while smoothing out homogeneous regions. In terms of the numerical implementation, three finite difference schemes, explicit, semi-implicit, and implicit are investigated. Experiments of denoising and restoration of synthetic, natural, and texture images show the effectiveness of our model.

1.1 Local Fourth Order Models

We recall several local fourth order models previously introduced in [5,6,12]. Let $\Omega \subset \mathbb{R}^2$ be the image domain, $f : \Omega \to \mathbb{R}$ the given noisy image, and $u : \Omega \to \mathbb{R}$ the restored image.

The You-Kaveh regularizer [5] is

$$E^{YK}(u) = \int_\Omega g(|\Delta u|)\mathrm{d}x,$$

where the authors require $g(\cdot) \geq 0$, $g'(\cdot) > 0$, and its corresponding time-dependent Euler-Lagrange equation is

$$\frac{\partial u}{\partial t} = -\Delta(g'(|\Delta u|)\frac{\Delta u}{|\Delta u|}) = -\Delta(c(|\Delta u|)\Delta u).$$

Usually, set $c(\cdot) = \frac{1}{1+(\cdot/k)^2} = g'(\cdot)$ and k is a modulatory parameter, which is the edge-preserving function from [2] (the independent variable being now $|\Delta u|$ instead of $|\nabla u|$).

The Lysaker-Lundervold-Tai (LLT) regularizer [6] minimizes the total variation norm of $|\nabla u|$, and it is

$$E^{LLT}(u) = \int_\Omega (|u_{x_1x_1}| + |u_{x_2x_2}|)\mathrm{d}x.$$

Based on the LLT model, Wen *et al.* [12] proposed an adaptive LLT regularizer (ALLT) to better preserve structures in images. The ALLT fourth-order model is the time-dependent gradient descent of the energy

$$E^{ALLT}(u) = \int_\Omega \alpha(f)(|u_{x_1x_1}| + |u_{x_2x_2}|)\mathrm{d}x,$$

where $\alpha(f) = \frac{1}{1+(\nabla f_\sigma/k)^2}$ is a feature detection function based on the gradient of the noisy image, and $f_\sigma = G_\sigma * f$, with $G_\sigma = \frac{1}{2\pi\sigma^2} e^{-\frac{\|x\|^2}{2\sigma^2}}$. From [7] and [12], gradient-based edge detector is more effective than second order derivative based.

These fourth order models encourage piecewise planar solutions [5,12]. Thus, these models can preserve edges without the staircase effect.

1.2 Nonlocal Total Variation (NLTV)

Nonlocal methods are well adapted to texture preserving and denoising. Referred to [9], we first review nonlocal differential operators. The nonlocal gradient vector $\nabla_w u(x) : \Omega \to \Omega \times \Omega$, is defined by

$$(\nabla_{NL} u)(x, y) := (u(y) - u(x))\sqrt{w(x, y)},$$

where $w : \Omega \times \Omega \to \mathbb{R}$ is a nonnegative and symmetric weight function, such as $w(x, y) = \exp\left\{-\frac{G_\sigma * (\|u(x+\cdot)-u(y+\cdot)\|^2)(0)}{2h^2}\right\}$. And the magnitude of nonlocal gradient at $x \in \Omega$ is

$$|\nabla_{NL} u|(x) = \sqrt{\int_\Omega (u(y) - u(x))^2 w(x, y) \mathrm{d}y}.$$

The nonlocal divergence $\mathrm{div}_{NL}\vec{v} : \Omega \times \Omega \to \Omega$ of the vector $\vec{v} : \Omega \times \Omega \to \mathbb{R}$ is defined as the adjoint of the nonlocal gradient

$$(\mathrm{div}_{NL}\vec{v})(x) := \int_\Omega (v(x, y) - v(y, x))\sqrt{w(x, y)}\mathrm{d}y.$$

The nonlocal Laplacian $\Delta_{NL} u : \Omega \to \mathbb{R}$ of u can be defined by

$$\Delta_{NL} u(x) := \frac{1}{2}\mathrm{div}_{NL}(\nabla_{NL} u(x)) = \int_\Omega (u(y) - u(x)) w(x, y)\mathrm{d}y.$$

Based on the above nonlocal operators, the NLTV regularization [9] is,

$$\min_u E^{NLTV}(u) = \int_\Omega |\nabla_{NL} u|,$$

and the associated time-dependent Euler-Lagrange equation is

$$\frac{\partial u}{\partial t} = \int_\Omega (u(y) - u(x)) w(x, y) \left(\frac{1}{|\nabla_{NL} u(x)|} - \frac{1}{|\nabla_{NL} u(y)|}\right) \mathrm{d}y,$$

which can also be expressed as

$$\frac{\partial u}{\partial t} = \mathrm{div}_{NL}\left(\frac{\nabla_{NL} u}{|\nabla_{NL} u|}\right).$$

2 The Proposed Model

Inspired by the local fourth order models and the nonlocal gradient and Laplacian, we propose the following nonlocal second order functional for image restoration,

$$\inf_u E(u) = \int_\Omega \alpha_{NL}(f)|\Delta_{NL}u|^2 \mathrm{d}x + \frac{\lambda}{2}\int_\Omega (f-Ku)^2 \mathrm{d}x, \tag{1}$$

where $|\Delta_{NL}u(x)| = |\int_\Omega (u(y)-u(x))w(x,y)\mathrm{d}y|$, $\alpha_{NL}(f)$ is an adaptive coefficient function to distinguish edges and smooth areas and thus will adaptively guide the image restoration process. The first term in (1) is the regularization term, while the second term is the usual data fidelity term; $K : L^2(\Omega) \to L^2(\Omega)$ models the blur kernel which is a linear and continuous operator, $\Omega \subset \mathbb{R}^2$ is the image domain, $f \in L^2(\Omega)$ is the given noisy-blurry image, and $\lambda > 0$ is a coefficient that balances the regularization and data fidelity terms.

The corresponding Euler-Lagrange equation associated with (1), in a time-dependent fashion, is

$$\frac{\partial u}{\partial t} = -\Delta_{NL}(\alpha_{NL}(f)\Delta_{NL}u) + \lambda K^*(f-Ku). \tag{2}$$

In the following, two choices of $\alpha_{NL}(f)$ are given.

The first one is $\alpha_{NL}(f) = 1$. The model (1) is isotropic, and the regularization term becomes a nonlocal biharmonic model. Fourth order linear diffusion damps oscillations at high frequencies much faster than second-order diffusion [13]. At the same time, different from second order based methods, fourth order methods can efficiently overcome the staircase effect, while preserving slopes and creases in the image.

The second one is

$$\alpha_{NL}(f) = \frac{1}{1+|\nabla_{NL}f_\sigma|^2/k^2}, \tag{3}$$

where k is a modulatory parameter, and as before, $f_\sigma = G_\sigma * f$ is a smoothed version of f. Using (3), model (1) becomes anisotropic, and $\alpha_{NL}(f)$ provides a guidance for the degree of diffusion. We use f_σ to first roughly removing the noise, and then utilize the nonlocal gradient $\nabla_{NL}f_\sigma$ as an edge detector. Thus, $\alpha_{NL}(f)$ has the ability of distinguishing edges and smooth areas of the original image. From the coefficient (3), $\alpha_{NL}(f) \in [0,1]$. On or near edges, $|\nabla_{NL}f_\sigma|$ is large and thus $\alpha_{NL}(f)$ is small approaching 0. On the contrary, on flat areas or away from edges, $|\nabla_{NL}f_\sigma|$ is small and $\alpha_{NL}(f)$ is large approaching 1. Using this coefficient (3) in the proposed high order functional (1), we have that $\alpha_{NL}(f)$ induces less diffusion when $|\nabla_{NL}f_\sigma|$ is large for preserving structures, and bigger diffusion when $|\nabla_{NL}f_\sigma|$ is small for smoothing out the noise.

Most of local fourth-order image restoration models use the second order derivatives (Laplace operator) to define the edge-preserving function to distinguish edges from homogeneous regions. Following [7] and [12], compared with the Laplace operator, the gradient operator has a better edge detection capability.

It is the same in nonlocal situations, and that is why we employ the nonlocal gradient for designing the adaptive coefficient function α (and not the nonlocal Laplacian). In the following, we give a group of simulation experiments to verify the above phenomenon.

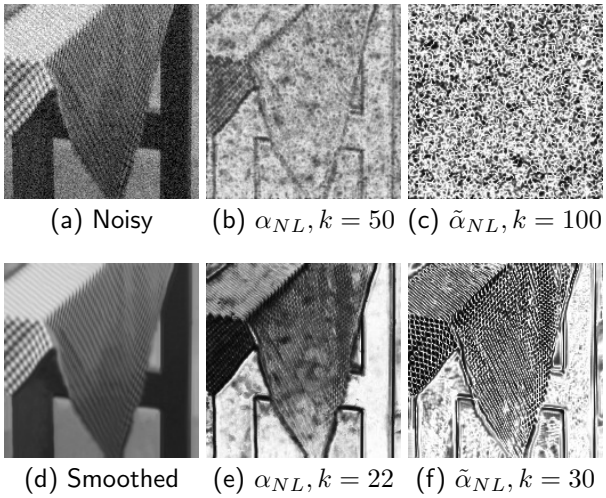

Fig. 1. Comparison of the edge detection ability of nonlocal gradient and nonlocal Laplace operator. (a) an noisy image, (b) α_{NL} for image (a) with $k = 50$, (c) $\tilde{\alpha}_{NL}$ for image (a) with $k = 100$, (d) a smoothed image, (e) α_{NL} for image (d) with $k = 22$, (f) $\tilde{\alpha}_{NL}$ for image (d) with $k = 30$.

Define the nonlocal Laplace operator based adaptive function by

$$\tilde{\alpha}_{NL}(f) = \frac{1}{1 + |\Delta_{NL} f_\sigma|^2 / k^2}. \tag{4}$$

For a fair comparison, the parameter k for both (3) and (4) is turned to best show the edges. First, we start with a noisy image f, and use (3) and (4) to distinguish edges and homogeneous areas. In Fig. 1(a), we show the noisy image. Correspondingly, Fig. 1(b) and Fig. 1(c) display the map of gradient-based and Laplace-based function, respectively. However, from Fig. 1(c) we can not find the roughly sharp edges of Fig. 1(a). Thus, as in the case of the local Laplace operator, the nonlocal Laplace operator cannot detect edges for images with a lot of noise. Second, there is another group of experiment in the second row of Fig. 1. Different from the first row, we replace f_σ with a smooth and cleaner image in (3) and (4). The edge maps of (3) and (4) are shown in Fig. 1(e) and Fig. 1(f), respectively. At the thick sharp edges, α_{NL} shows dark lines. On the contrary, as expected, $\tilde{\alpha}_{NL}$ shows two light lines at the boundary of edges. It verifies the bilateral effect of the nonlocal Laplace operator, which is the same as

when using the local version. Also, the nonlocal Laplace based edge detector has a larger reaction of crease points (such as the table leg of Fig. 1(f)). Thus, the nonlocal gradient based function is more suitable for distinguishing edges and homogeneous areas.

3 Numerical Implementation

To numerically solve the proposed model (1), we design three different finite difference schemes. Before introducing these three schemes, we first give some notations.

Let u_i^n denote the value of a pixel i in the image ($1 \leq i \leq N$) with time level n, the time step is τ, $t = n\tau$, $n = 0, 1, ...$, and let $w_{i,j}$ be the sparsely discrete version of $w = w(x, y) : \Omega \times \Omega \to \mathbb{R}$. We use the neighbors set $j \in N_i$ defined by $j \in N_i := \{j : w_{i,j} > 0\}$. Then, as in [9], the discretizations of the nonlocal gradient $\nabla_{NLd}(u_i)$ and nonlocal Laplacian $\Delta_{NLd}(u_i)$ are

$$\begin{aligned} \nabla_{NLd}(u_i) &:= (u_j - u_i)\sqrt{w_{i,j}}, \quad j \in N_i, \\ \Delta_{NLd}(u_i) &:= \sum_{j \in N_i} (u_j - u_i) w_{i,j}, \end{aligned}$$

and the magnitude of the discrete nonlocal gradient is

$$|\nabla_{NLd}(u_i)| := \sqrt{\sum_{j \in N_i} (u_j - u_i)^2 w_{i,j}}. \tag{5}$$

We construct the weight function $w_{i,j}$ following the algorithm in [9,11].

Explicit Scheme We first give the finite difference explicit scheme, as follows,

$$\frac{u_i^{n+1} - u_i^n}{\tau} = -\Delta_{NLd}(\alpha_{NL}(f_i)\Delta_{NLd}(u_i^n)) + K^*(f_i - Ku_i^n). \tag{6}$$

Implicit Scheme The implicit scheme is

$$\frac{u_i^{n+1} - u_i^n}{\tau} = -\Delta_{NLd}(\alpha_{NL}(f_i)\Delta_{NLd}(u_i^{n+1})) + K^*(f_i - Ku_i^n). \tag{7}$$

Semi-implicit Scheme For the semi-implicit scheme, we first expand the proposed fourth order regularizer as

$$-\Delta_{NL}(\alpha_{NL}(f)\Delta_{NL}u) = -\int_\Omega \left(\alpha_{NL}(f)(y)\Delta_{NL}u(y) - \alpha_{NL}(f)(x)\Delta_{NL}u(x)\right) w(x, y)\mathrm{d}y,$$

where $\Delta_{NL}u(y) = \int_\Omega (u(z) - u(y))w(y,z)\mathrm{d}z$ and $\Delta_{NL}u(x) = \int_\Omega (u(z') - u(x))w(x,z')\mathrm{d}z'$. Thus, the regularization term equals to

$$\begin{aligned} &- \int_\Omega \alpha_{NL}(f)(y) \cdot \int_\Omega (u(z) - u(y))w(y,z)\mathrm{d}z \cdot w(x,y)\mathrm{d}y \\ &\qquad + \int_\Omega \alpha_{NL}(f)(x) \cdot \int_\Omega u(z')w(x,z')\mathrm{d}z' \cdot w(x,y)\mathrm{d}y \\ &\qquad\qquad - \alpha_{NL}(f)(x) \cdot u(x) \int_\Omega \int_\Omega w(x,z')\mathrm{d}z' \cdot w(x,y)\mathrm{d}y. \end{aligned}$$

Notice, the u in the last term of the above formula is independent of the integration, and we discretize it in the $n+1$ level. Therefore, the semi-implicit scheme is,

$$\begin{aligned} &\frac{u_i^{n+1} - u_i^n}{\tau} + \alpha_{NL}(f_i) \cdot u_i^{n+1} \sum_{j \in N_j} (w_{i,j} \sum_{k \in N_k} w_{i,k}) \\ &= - \sum_{j \in N_j} \alpha_{NL}(f_j) \Delta_{NLd}(u_j^n) + \alpha_{NL}(f_i) \sum_{j \in N_j} \sum_{k' \in N_k'} (u_{k'}^n w_{i,j} \cdot w_{i,k'}) + K^*(f_i - K u_i^n). \end{aligned} \tag{8}$$

For the explicit scheme (6) and semi-implicit scheme (8), u_i^{n+1} can be expressed explicitly. However, for the implicit scheme (7), the inverse of a very large matrix has to be calculated to solve for u_i^{n+1}.

4 Experiments

In order to quantify the denoising and restoration effect, for the original clean image u_{O} and its restored image u, the denoising performance is measured in terms of peak signal to noise ratio (PSNR),

$$\mathrm{PSNR} = 10\log_{10} \frac{M_1 N_1 |\max u_{\mathrm{O}} - \min u_{\mathrm{O}}|}{\|u - u_{\mathrm{O}}\|_{L^2}^2} \mathrm{dB},$$

and mean absolute deviation error (MAE),

$$\mathrm{MAE} = \frac{\|u - u_{\mathrm{O}}\|_{L^1}}{M_1 N_1},$$

where $M_1 \times N_1$ is the size of image. Besides, we also use the structural similarity (SSIM) [14].

4.1 Image Denoising

We apply our proposed model to image denoising, and thus this is when the blur kernel K is the identity. To study the performance of our method, we compare the proposed NLABH model (1) with ALLT [12] and NLTV [9]. For illustration,

we test four images *synthetic*, *Lena*, *Barbara*, and *texture* (the original images are shown in Fig. 3 and Fig. 4).All the Denoising results obtained using the NLABH model are obtained using the semi-implicit scheme. The PSNR, MAE, and SSIM values of the Denoising results are listed in Table 1, where the best results are shown in boldface. Next, we report some of the numerical experiments for the original test images and the corresponding results are depicted in Fig. 3 and Fig. 4.

Table 1. Comparison of PSNR, MAE, and SSIM of the different models with Gaussian noise, and noise level $\sigma_{\mathrm{n}} = 10, 20, 30$.

	PSNR			MAE			SSIM		
σ_{n}	10	20	30	10	20	30	10	20	30
synthetic									
ALLT	**43.820**	**38.548**	35.045	1.058	1.767	2.869	0.507	0.448	0.418
NLTV	42.074	36.921	35.042	0.964	1.906	2.419	**0.765**	**0.481**	**0.450**
NLABH	42.775	38.224	**35.323**	**0.824**	**1.531**	**2.273**	0.752	0.470	0.439
Lena									
ALLT	33.611	29.892	27.953	3.748	5.506	6.820	0.744	0.630	0.552
NLTV	34.562	30.820	28.802	3.458	5.151	6.455	0.743	0.630	0.559
NLABH	**34.992**	**31.464**	**29.348**	**3.250**	**4.735**	**6.045**	**0.768**	**0.663**	**0.583**
Barbara									
NLTV	34.371	30.377	28.575	3.633	5.648	6.863	0.724	0.601	0.521
NLABH	**35.046**	**31.729**	**29.619**	**3.359**	**4.803**	**6.164**	**0.757**	**0.661**	**0.572**
texture									
NLTV	**29.419**	**24.907**	22.671	**6.830**	**11.439**	14.868	0.950	0.859	0.774
NLABH	29.315	24.806	**22.689**	6.880	11.472	**14.567**	**0.951**	**0.866**	**0.792**

Fig. 2 shows the energy (1) with time for two experiments, and $\lambda = 0.1$, $\tau = 0.001$. The energy values for both experiments are continuously decreasing and eventually stabilize, which illustrates the stability of our numerical scheme in practice.

For the synthetic image in first row of Fig. 3 containing smooth surfaces and sharp edges, the local fourth order model ALLT [12] can restore the smooth areas while preserve edges very well, which corresponds to the property of fourth order equations. Comparing the NLTV and NLABH, the first row of Fig. 3 and Table 1 show that NLABH can restore homogeneous regions smoothly, and the shape of edges is preserved sharply due to the adaptive function.

For the real image *Lena* (the second row of Fig. 3), the best denoised image is the one denoised by NLABH, both visually and by measurements. The NLABH model can better preserve both sharp and blunt lines in the image. Fig. 4 shows denoising results of texture images (*Barbara* and *texture*). Because the local method does not work well in textured regions, we only show the results of NLTV and NLABH. The denoised images by NLABH are smoother; simultaneously, texture and edges are preserved. Moreover, we can still see a little bit of the

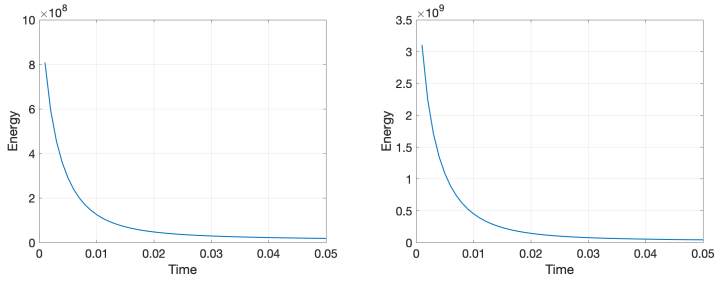

Fig. 2. Energy versus time for denoising experiments. (left) *Lena* with $\sigma_{\mathrm{n}} = 20$, (right) *Barbara* with $\sigma_{\mathrm{n}} = 10$.

Fig. 3. Denoising results of *synthetic* and *Lena* images. The first column: (top) original image *synthetic*, (bottom) original image *Lena*. The second column: (top) noisy image for *synthetic* image, $\sigma_{\mathrm{n}} = 20$, (bottom) *Lena* image, $\sigma_{\mathrm{n}} = 10$. The third-fifth columns: denoised images using ALLT, NLTV, and NLABH methods.

staircase effect in the denoised images using NLTV. From the second row of Fig. 4 (*Barbara*), compared with NLTV, NLABH can restore these blunt texture at the upper part of the tablecloth. All of these verify the effectiveness of NLABH.

4.2 Image Restoration

In this subsection, we compare the NLTV and NLABH models for image restoration. The algorithm details of NLTV for image restoration is given in [10]. As for the denoising experiments from subsection 4.1, we employ the semi-implicit scheme and give PSNR, MAE, and SSIM values for comparison.

Simulation experiment results are shown in Fig. 6. The corresponding comparison of PSNR, MAE, and SSIM is listed in Table 2. We show the energy (1) of time for two experiments. λ in Fig. 5 is 16 and 250 respectively, and $\tau = 0.1$. The energy values decrease with time, which shows that the algorithm for numerically solving our model ((1)) is stable in practice. From the first row of Fig. 6, we can see that the proposed NLABH model has a good performance at restoring the curved surface. Moreover, the restored images obtained using the NLABH

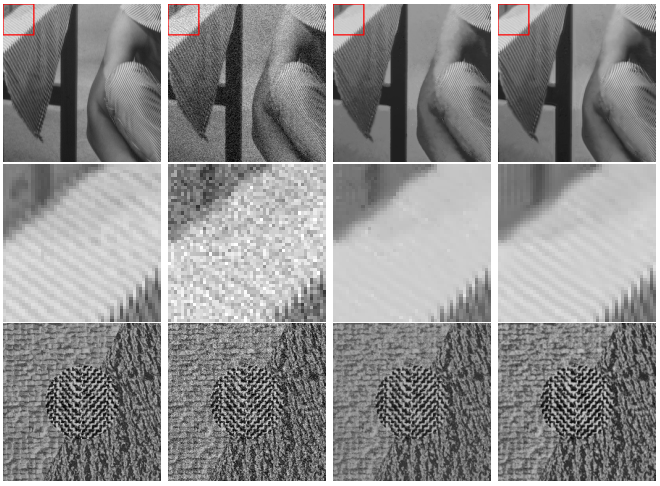

Fig. 4. Denoising results of *Barbara* and *texture* images. The first column: (top) original image *Barbara*, (middle) zoom in part of *Barbara* corresponding to the red box, (bottom) original image *texture*. The second column: (top) noisy image for *Barbara* image, $\sigma_{\mathrm{n}} = 20$, (middle) zoom in part of noisy *Barbara* corresponding to the red box, (bottom) *texture* image, $\sigma_{\mathrm{n}} = 30$. The third-fourth columns: denoised images using NLTV and NLABH methods.

model are cleaner than the ones obtained by the NLTV. From the second row of Fig. 6, the lines restored by NLABH are more fluent without serrated edges. At the same time, the third and fourth rows of Fig. 6 verify the effectiveness of preserving fluent lines.

5 Conclusion

We have proposed in this paper an anisotropic nonlocal fourth order biharmonic model for image denoising and restoration. We have discretized the model using finite difference schemes that are stable in practice. We have presented numerous experimental results on synthetic and real images that show the advantages of the proposed model, by comparison with local fourth order models and nonlocal second order models. We have also shown through experiments that the nonlocal gradient is better suited for edge detection than the nonlocal Laplacian. Future work will provide further analysis of the model and investigate other applications.

References

1. Leonid I Rudin, Stanley Osher, and Emad Fatemi. Nonlinear total variation based noise removal algorithms. *Physica D: nonlinear phenomena*, 60(1-4):259–268, 1992.
2. Pietro Perona and Jitendra Malik. Scale-space and edge detection using anisotropic diffusion. *IEEE Transactions on pattern analysis and machine intelligence*, 12(7):629–639, 1990.

Table 2. Comparison of PSNR, MAE, and SSIM of the different models with different blur and noise

	Gaussian blur σ_b	Gaussian noise σ_n	Model	PSNR	MAE	SSIM
synthetic	2	7	NLTV	**35.023**	**1.876**	**0.858**
			NLABH	34.505	2.249	0.438
Lena	2	7	NLTV	**27.909**	6.347	0.565
			NLABH	27.897	**6.294**	**0.585**
Barbara-1	1	7	NLTV	21.211	17.263	**0.276**
			NLABH	**21.421**	**16.477**	0.266
Barbara-2	1	10	NLTV	26.048	9.075	**0.427**
			NLABH	**26.198**	**8.768**	0.420

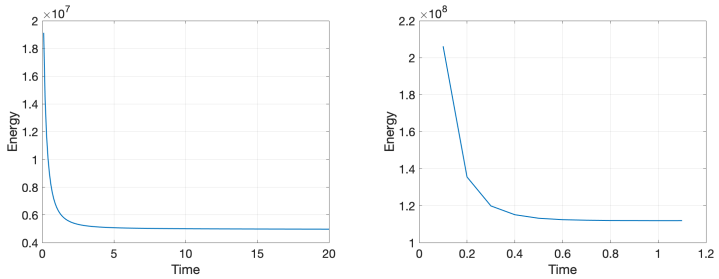

Fig. 5. Energy versus time for restoration experiments. (left) *synthetic* with $\sigma_b = 2$, $\sigma_n = 7$, (right) *Barbara-1* with $\sigma_b = 1$, $\sigma_n = 7$.

3. Antonin Chambolle and Pierre-Louis Lions. Image recovery via total variation minimization and related problems. *Numerische Mathematik*, 76(2):167–188, 1997.
4. Tony Chan, Antonio Marquina, and Pep Mulet. High-order total variation-based image restoration. *SIAM Journal on Scientific Computing*, 22(2):503–516, 2000.
5. Y-L You and Mostafa Kaveh. Fourth-order partial differential equations for noise removal. *IEEE Transactions on Image Processing*, 9(10):1723–1730, 2000.
6. Marius Lysaker, Arvid Lundervold, and Xue-Cheng Tai. Noise removal using fourth-order partial differential equation with applications to medical magnetic resonance images in space and time. *IEEE Transactions on image processing*, 12(12):1579–1590, 2003.
7. Mohammad Reza Hajiaboli. A self-governing hybrid model for noise removal. In *Pacific-Rim Symposium on Image and Video Technology*, pages 295–305. Springer, 2009.
8. Antoni Buades, Bartomeu Coll, and J-M Morel. A non-local algorithm for image denoising. In *2005 IEEE Computer Society Conference on Computer Vision and Pattern Recognition (CVPR'05)*, volume 2, pages 60–65. IEEE, 2005.
9. Guy Gilboa and Stanley Osher. Nonlocal operators with applications to image processing. *Multiscale Modeling & Simulation*, 7(3):1005–1028, 2009.
10. Yifei Lou, Xiaoqun Zhang, Stanley Osher, and Andrea Bertozzi. Image recovery via nonlocal operators. *Journal of Scientific Computing*, 42(2):185–197, 2010.

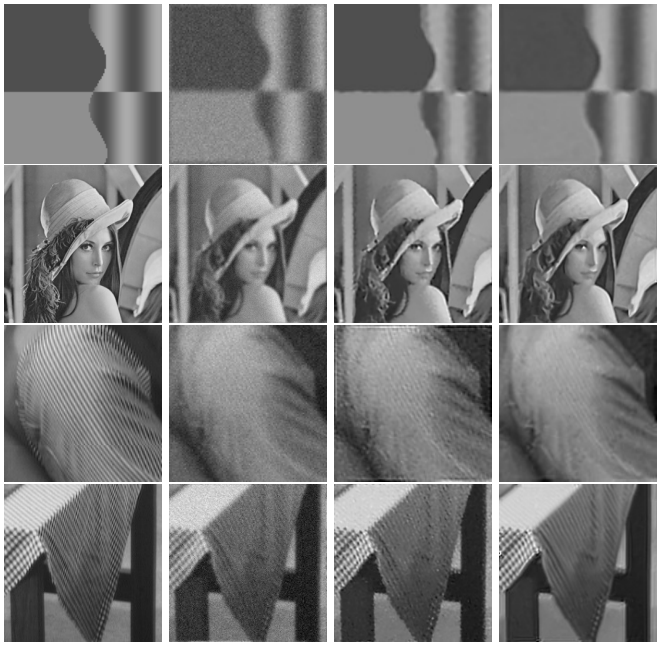

Fig. 6. Restoration results. The first column: original images *synthetic*, *Lena*, *Barbara-1*, and *Barbara-2* from top to bottom. The second column: blurry and noisy images, *synthetic*: $\sigma_b = 2$, $\sigma_n = 7$, *Lena*: $\sigma_b = 2$, $\sigma_n = 7$, *Barbara-1*: $\sigma_b = 1$, $\sigma_n = 7$, *Barbara-2*: $\sigma_b = 1$, $\sigma_n = 10$. The third-fourth columns: restored images by NLTV and NLABH.

11. Miyoun Jung, Xavier Bresson, Tony F Chan, and Luminita A Vese. Nonlocal mumford-shah regularizers for color image restoration. *IEEE transactions on image processing*, 20(6):1583–1598, 2010.
12. Ying Wen, Jiebao Sun, and Zhichang Guo. A new anisotropic fourth-order diffusion equation model based on image feature for image denoising. *CAM report*, 2020.
13. Andrea L Bertozzi and John B Greer. Low-curvature image simplifiers: Global regularity of smooth solutions and laplacian limiting schemes. *Communications on Pure and Applied Mathematics: A Journal Issued by the Courant Institute of Mathematical Sciences*, 57(6):764–790, 2004.
14. Zhou Wang, Alan C Bovik, Hamid R Sheikh, and Eero P Simoncelli. Image quality assessment: from error visibility to structural similarity. *IEEE transactions on image processing*, 13(4):600–612, 2004.